DE GRUYTER Z. Naturforsch. 2025; 80(11–12)b: 413–423

Tehzeeb Sawaira, Amna Jamil, Zuraiz Ahmad Khan, Ahsan Sharif, Maha Alruwaili, Asghar Ali
and Adeel Afzal*

Flower-like assembly of single-phase V–TiO$_2$ microneedles for sustainable water remediation

https://doi.org/10.1515/znb-2025-0037
Received May 18, 2025; accepted July 15, 2025;

Abstract: Designing efficient photocatalysts that operate under sunlight is critical for sustainable water remediation. This work presents the synthesis of flower-like assemblies of single-phase vanadium-doped titanium dioxide (V–TiO$_2$) microneedles via a simple sol-gel method. The engineered microneedle architecture offers enhanced surface area and light-scattering properties, while the substitutional doping of V^{5+} ions into the TiO$_2$ structure results in significant bandgap narrowing (3.13 eV) and suppressed electron-hole recombination. Comprehensive structural and surface analyses were performed using X-ray diffraction, scanning electron microscopy, Fourier-transform infrared, and UV/vis spectroscopy. Photocatalytic studies under UV and sunlight conditions reveal that thermally annealed V–TiO$_2$ (ΔV-TiO$_2$) achieves 80 % degradation of methylene blue (MB), markedly outperforming undoped TiO$_2$. The photocatalytic reaction follows pseudo-first-order kinetics with a rate constant of 1.7×10^{-2} min^{-1}, approximately four times higher than that of annealed pristine TiO$_2$ (ΔTiO$_2$). The enhanced activity is attributed to improved charge separation and redox dynamics introduced by vanadium incorporation. These findings demonstrate the effectiveness of ΔV-TiO$_2$ microneedles as highly active, sunlight-driven photocatalysts for the degradation of organic contaminants in wastewater.

Keywords: titanium dioxide; v-doped; photocatalysis; environmental remediation; wastewater treatment

1 Introduction

Revolutionary developments of the 20th century have accelerated economic growth but have inadvertently contributed to the enormous rise in air and water pollution.[1] The industrial focus on producing commercial goods frequently leads to the careless emancipation of hazardous byproducts into water streams, including pharmaceuticals, pesticides, fertilizers, dyes, and other emerging organic contaminants.[2,3] The ingression of these toxins in the food chain and drinking water poses a serious threat to human health. For example, organic coloring compounds (dyes) released by the textile industry, such as methylene blue, are harmful to aquatic life, plants, animals, and humans.[4,5]

Therefore, it is crucial to treat the wastewater coming from industries by removing the harmful organic contaminants from it, to ensure a cleaner and safer environment.[6] Among the various treatment methods, the sunlight-assisted photocatalytic removal of organic pollutants is an effective strategy to treat wastewater.[7,8] In these techniques, TiO$_2$ nanostructures have received a lot of attention as photocatalysts for the removal of organic pollutants due to their chemical and thermal stability, biocompatibility, cost efficiency, and exceptional oxidizing capability.[9,10] TiO$_2$-based photocatalysis, however, suffers some drawbacks, including their low hydrophobic organic pollutant adsorption capacity, high photogenerated electron and hole recombination rate, and decreased photocatalytic efficacy of pure TiO$_2$ nanostructures under sunlight.

To overcome these restraints, various methods are proposed, including the incorporation of *n*-type or *p*-type dopants into or within TiO$_2$ structures, which may reduce the band gap and lower the recombination rate of electron-hole pairs.[11,12] Vanadium cations, in this situation, have shown a great ability to improve the photocatalytic activities of nanomaterials like TiO$_2$, ZrO$_2$, etc.[13–15] For instance, Yao et al.[16] produced V-doped TiO$_2$ nanoparticles of the anatase type using a sol-gel method, with reduced bandgap energy and enhanced photocatalytic elimination of acid yellow 36 dye under sunlight. Recently, Nguyen et al.[14] also demonstrated high photodegradation activity of hydrothermally synthesized mixed-phase V–TiO$_2$ photocatalysts for trichloroethylene. They confirmed the incorporation of V^{5+} and V^{4+}

***Corresponding author: Adeel Afzal**, School of Chemistry, University of the Punjab, Quaid-i-Azam Campus, Lahore, 54590, Pakistan, E-mail: adeel.chem@pu.edu.pk
Tehzeeb Sawaira, Amna Jamil, Zuraiz Ahmad Khan and Ahsan Sharif, School of Chemistry, University of the Punjab, Quaid-i-Azam Campus, Lahore, 54590, Pakistan, E-mail: qandeel.un.nisa@gmail.com (T. Sawaira), amnajamil205@gmail.com (A. Jamil), zuraiz77@gmail.com (Z.A. Khan), ch.ahsan.chem@pu.edu.pk (A. Sharif)
Maha Alruwaili, Department of Physics, College of Science, University of Hafr Al Batin, Hafr Al Batin, 39524, Saudi Arabia, E-mail: maalruwaili@uhb.edu.sa
Asghar Ali, Department of Chemistry, College of Science, University of Hafr Al Batin, Hafr Al Batin, 39524, Saudi Arabia, E-mail: asgharali@uhb.edu.sa

ions into the TiO_2 structure, resulting in substitutional doping, and ascribed the reduction in bandgap to the presence of V^{4+} states.[14]

Recent studies have suggested that incorporation of vanadium into the TiO_2 structure can introduce localized V^{5+} energy states within the band gap, which interact with the Ti^{4+} electronic states and reduce the effective band gap by facilitating charge transfer through these dopant-induced states.[16] Regardless of substantial research into V-doping as an efficient method to enhance the catalytic activity, the fundamental structural and morphological aspects of V–TiO_2 nanostructures need to be further understood. Also, there is a need to create novel morphologically distinct V–TiO_2 nanostructures to investigate their influence on the aerobic photodegradation of environmental pollutants.

We report the synthesis of V–TiO_2 microneedles assembled into flower-like morphology with phase-pure anatase structure and excellent photocatalytic properties for the elimination of methylene blue (MB) dye under UV and sunlight irradiation. The impact of V^{5+} doping, calcination, crystal structure, and surface chemistry on the performance of V–TiO_2 microneedles is investigated. The photocatalytic performance of the V–TiO_2 microneedles is also compared with pure anatase TiO_2 nanoparticles as a reference. As a result, the V–TiO_2 photocatalytic system is highly efficient in the degradation of organic contaminants from wastewater, ensuring a sustainable approach to water purification.

2 Experimental

2.1 Synthesis of pure TiO_2

Pristine TiO_2 was synthesized by dissolving 1 g (2.74 mmol) of cetyltrimethylammonium bromide (CTAB, extra pure, Oxford Lab) in 20 mL of isopropanol (*iso*-PrOH, ≥99.8 %, Sigma-Aldrich) in a 100 mL beaker, followed by stirring for 15 min. Subsequently, 5 mL (4.7 g, 13.8 mmol) of titanium *n*-butoxide ($Ti(On\text{-}Bu)_4$, ≥99 %, Alfa Aesar, liquid) was added to the solution under continuous stirring for 1 h at room temperature. Distilled water was then added dropwise in a 4:1 ratio relative to CTAB. The mixture was stirred for 3–4 h at 60 °C and then left at room temperature for 24 h. TiO_2 precipitates were formed and separated.

2.2 Synthesis of V–TiO_2

V-doped TiO_2 was prepared by taking 175 mg (0.962 mmol) of vanadium oxide (V_2O_5, ≥99.5 %, Riedel-de Haën) in 20 mL isopropanol, followed by 15 min of stirring. Next, 1 g of CTAB was added and the mixture stirred for 15 min. After that, 3 mL of $Ti(On\text{-}Bu)_4$ was added, and the mixture was stirred for 1 h. Distilled water (4 mL) was added in a 4:1 (weight ratio) with respect to CTAB, and stirring was continued for 3–4 h at 60 °C. Afterwards, the reaction mixture was left at room temperature for 24 h. Precipitates of V–TiO_2 were separated, thoroughly washed, and dried in an oven at 60 °C. Yield of V–TiO_2 was ~0.5 g. Half (0.25 g) of both the prepared pristine TiO_2 and the V–TiO_2 samples were calcined at 45 °C for 4 h to analyze structural changes and enhance photocatalytic properties by removing surface impurities. The calcined forms are labeled as ΔTiO_2 and $\Delta V\text{-}TiO_2$.

2.3 Characterization

The structural analyses of the prepared photocatalysts were performed by X-ray diffractometry (XRD). For Fourier Transform infrared spectroscopy (FTIR) an Agilent Cary 630 spectrophotometer was used and for UV/vis the double-beam spectrophotometer APEL PD-303. The surface morphology was studied using FEI Inspect S50 scanning electron microscopy (SEM).

2.4 Photocatalysis study

The photocatalysis study of the as-prepared and calcined samples was carried out under UV light (30 W UV lamp) and natural sunlight for the removal of methylene blue. The photocatalysts (30 mg) were taken in an aqueous solution of methylene blue (5 ppm, 30 mL) and stirred in the dark for 60 min to establish adsorption/desorption equilibrium. After that, 4 mL of each sample solution was taken and the progress of MB degradation was monitored using UV/vis spectrophotometer by measuring the absorbance at λ = 665 nm for different time intervals. The percentage degradation of the pollutant was evaluated using Equation (1).

$$\text{Dye degradation}\,(\%) = \frac{C_0 - C_t}{C_0} \times 100 \qquad (1)$$

where C_o represents the initial concentration, while C_t refers to the concentration of methylene blue at a specific time (t). The reaction kinetics and rate constants of the photodegradation study were estimated by using the pseudo-first-order kinetic Equation (2).

$$k\,t = -\ln\left(C_t / C_o\right) \qquad (2)$$

A graph was plotted between $-\ln(C_t/C_o)$ and time (t). A straight line was obtained. The R^2 value close to one proves that our samples follow pseudo-first-order kinetics and the

Langmuir-Hinshelwood model. The slope of the straight line gives the value of the rate constant *k* which is obtained from the calibration plot.

3 Results and discussions

3.1 Surface morphology

The SEM micrographs shown in Figure 1 illustrate the distinct surface morphology of the vanadium-doped TiO_2 (V–TiO_2) photocatalyst at two magnification levels. The low-magnification image (1,000 ×) reveals a homogeneous distribution of densely packed, spherical, and irregular agglomerates across the substrate. These agglomerates appear to be composed of finer nanostructured features, indicating a hierarchical assembly at the microscale. The spatial uniformity and dense surface coverage suggest effective nucleation and growth during the sol-gel synthesis process, which is crucial for ensuring consistent photocatalytic activity over a large area.[17] The inset, recorded at a higher magnification of 20,000 × , reveals the detailed internal morphology of the individual agglomerates, showcasing a highly organized flower-like architecture composed of radially aligned microneedles. These microneedles are slender, elongated structures that radiate outward from a central core, forming a three-dimensional network. The needle-like projections provide an extensive surface area and interstitial voids, which are advantageous for enhanced light harvesting and greater accessibility of active sites during photocatalytic degradation processes.[18,19] The high degree of orientation and tight packing of these microneedles also indicates robust crystallite formation, potentially resulting from effective incorporation of V ions into the TiO_2 structure during synthesis. The formation of microneedle or nanorod morphologies in TiO_2 is a well-established outcome of hydrothermal and related synthetic methods, as documented in previous studies.[20] In our work, the V-doped TiO_2 samples also exhibited this characteristic microneedle structure, consistent with the reported morphology of undoped TiO_2. This observation indicates that vanadium incorporation occurs without disrupting the fundamental structural framework of TiO_2. The observed morphology should be able to support improved charge separation by facilitating direct pathways for electron transport and reducing bulk recombination.[21] Furthermore, the flower-like microstructure with sharp edges and high aspect-ratio microneedles can potentially enhance photon scattering, increasing the optical path length and thereby boosting photocatalytic efficiency under both UV and sunlight exposure.[22]

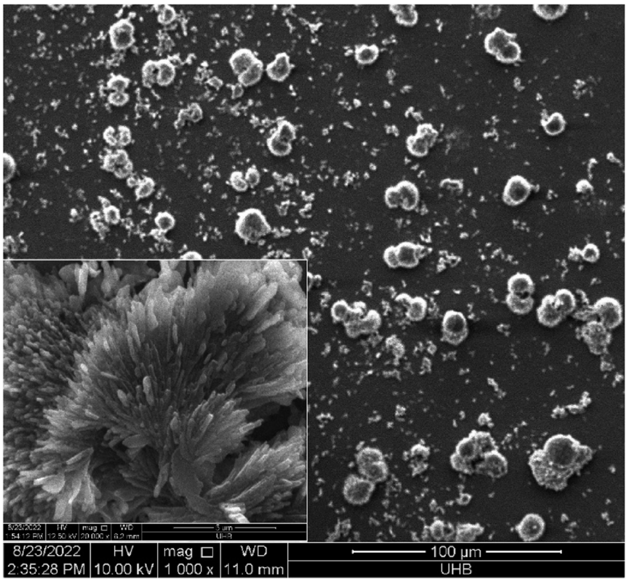

Figure 1: SEM images of ΔV-TiO_2 photocatalyst, showing the flower-like assembly of the ΔV-TiO_2 microneedles.

3.2 X-ray diffraction

For further structural characterization of the prepared photocatalysts, powder XRD was conducted, and the resulting patterns are shown in Figure 2. A prominent peak at 25.2° corresponds to the anatase (101) phase (JCPDS Card No. 21–1,272),[23,24] which confirms the formation of TiO_2. For comparison the XRD of pristine V_2O_5 was also done. At 20.31° an intense diffraction peak is observed which indexed to the (001) phase-pure plane of orthorhombic V_2O_5 (JCPDS Card No. 00-041-1,426),[25] confirming its structural identity. Apart from the (001) plane, additional diffraction peaks observed at $2\theta = 15.31$, 21.71, 26.08, 30.95, 32.38, and 34.22° are indexed to the (200), (101), (110), (301), (011), and (310) planes of orthorhombic V_2O_5,[26] being consistent with the standard JCPDS Card No. 00-041-1,426. These characteristic peaks of V_2O_5 are absent in the XRD pattern of as-prepared (TiO_2, V–TiO_2) and calcined (ΔTiO_2, ΔV-TiO_2) photocatalysts, indicating that the V^{5+} ions have been integrated into the TiO_2 structure, resulting in the formation of V-doped TiO_2 microneedles.[27] The crystallite size of the as-prepared and calcined photocatalysts was calculated using the Debye-Scherrer formula[28] for the (101) anatase phase. TiO_2 shows small peaks for a crystallite size of 4 nm, which increases to 6.8 nm in the case of ΔTiO_2 with higher intensity of the peaks. This shows that calcination causes an increase in the crystallite size.[29] In the case of V–TiO_2, the calculated crystallite size was 3.7 nm. However, the calcined ΔV-TiO_2 showed a relatively small increase in the crystallite size, i.e., 3.7–6.5 nm, which can be due to the growth-inhibiting effect of V^{5+} ions. The surface

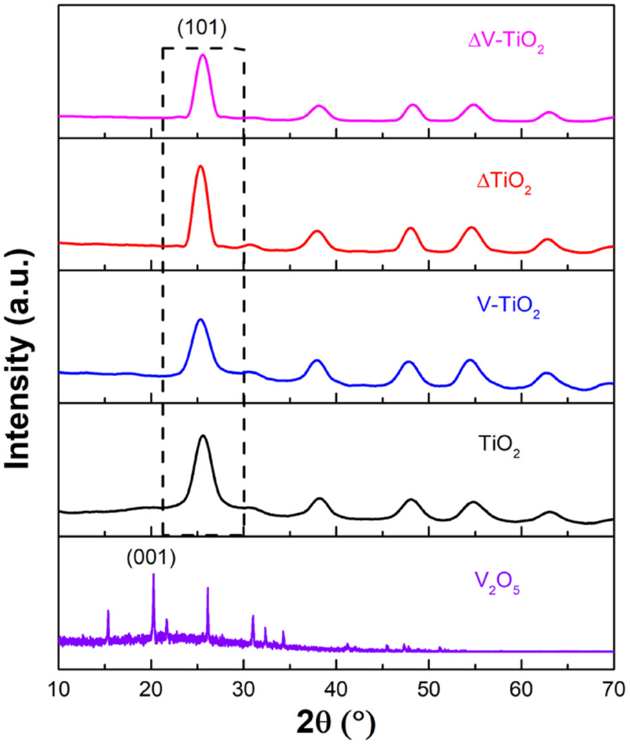

Figure 2: XRD patterns of pristine vanadium pentaoxide (V_2O_5), as-prepared (TiO_2, V–TiO_2) and calcined (ΔTiO_2, ΔV-TiO_2) photocatalysts.

confinement of V^{5+} in the structure could thus responsible for the reduction in the crystal size of calcined ΔV-TiO_2 as compared to the ΔTiO_2.[30] No peaks corresponding to rutile phase were observed in the XRD pattern of as-prepared and calcined photocatalysts, confirming that the samples consist of phase-pure anatase. A weak feature near 30° is sometimes reported in anatase systems and can arise from overlapping anatase reflections or background scattering, but it does not correspond to rutile. Thus, the microneedles are confirmed to be phase-pure anatase.

3.3 FTIR spectroscopy

The FTIR spectra of TiO_2 and calcined TiO_2 produced using CTAB as a precursor are shown in Figure 3. They allow assignments to the functional groups present in the compound. The stretching and deformations of the OH group are responsible for the wide absorption bands at 3,600 and 3,000 cm^{-1} and 1,645 and 1,631 cm^{-1}, respectively. These bands show that water molecules are poorly bonded to TiO_2. They restrict electron-hole pairs from recombining. This property is essential for photocatalysis.[31] Below 1,200 cm^{-1}, the wide, strong band is caused by Ti–O–Ti vibrations. The absorption bands at 763 cm^{-1} and 847 cm^{-1} are attributed to the stretching vibration of Ti–O–Ti, which is in agreement with the literature.[32]

The FTIR spectrum of pristine V_2O_5, V-doped TiO_2 and calcined V-doped TiO_2 are also shown in Figure 3. In the FTIR analysis of V_2O_5, the spectral region below 1,050 cm^{-1} is emphasized, as this region corresponds to the characteristic vibrational modes of various V–O bonding groups. An intense peak at 1,002 cm^{-1} is assigned to the V=O stretching vibrations [33] and a broad peak at 804 cm^{-1} is attributed to the V–O–V deformation mode.[34] The peaks at 711 cm^{-1} and 725 cm^{-1} of calcined and preheated V-doped TiO_2 correspond to the Ti–O–Ti stretching vibration. Around 815 cm^{-1} and 951 cm^{-1}, there are distinct absorption peaks which can be assigned to the symmetric stretching mode of V=O and the asymmetric stretching mode of V–O–V. These peaks were observed at 918 cm^{-1} and 824 cm^{-1} in the case of preheated V-doped TiO_2.[35] For better visualization of these peaks, a magnified view of the FTIR spectra in the <1,000 cm^{-1} range is shown in Figure 3(b). The stretching and deformation vibrations of O–H were observed at 3,374 cm^{-1} and 1,635 cm^{-1} in the spectrum of calcined V–TiO_2 and at 3,332 cm^{-1} and 1,630 cm^{-1} in the spectrum of preheated V–TiO_2. Because of the removal of residual organics and surface adsorbates during calcination, the spectrum of the calcined samples displayed fewer additional peaks.[35]

3.4 UV/vis measurements

The optical properties of the synthesized samples were investigated through UV/vis spectroscopy, and the spectra are shown in Figure 4. They provide crucial parameters for comparing the catalytic properties of the photocatalysts. Figure 4(a) shows the UV/vis absorption spectrum of pristine V_2O_5. It exhibits a sharp absorption band in the ultraviolet region, with the maximum absorption peak observed at 303 nm. This strong absorption in the ultraviolet region is associated with charge transfer transitions from O_2 p to V 3 d orbitals, which is characteristic behavior of transition metal oxides.[33] According to the literature, TiO_2 microneedles show absorption in the ultraviolet region.[36] All the photocatalysts showed maxima for the electronic transitions as shown in Figure 4(b–e). The maximum absorption of pristine TiO_2 was observed at 343 nm, which showed a redshift in the case of Δ$TiO_{2,}$ whose peak was at 350 nm. The doped samples, V–TiO_2 and ΔV-$TiO_{2,}$ showed absorption maxima at 348 nm and 356 nm, respectively, which lie in the absorption range of V–TiO_2. For ΔV-TiO_2, a minor shoulder appears in the 400–500 nm region after calcination, which can be ascribed to defect states or trace surface species introduced during thermal treatment. However, the overall absorption edge

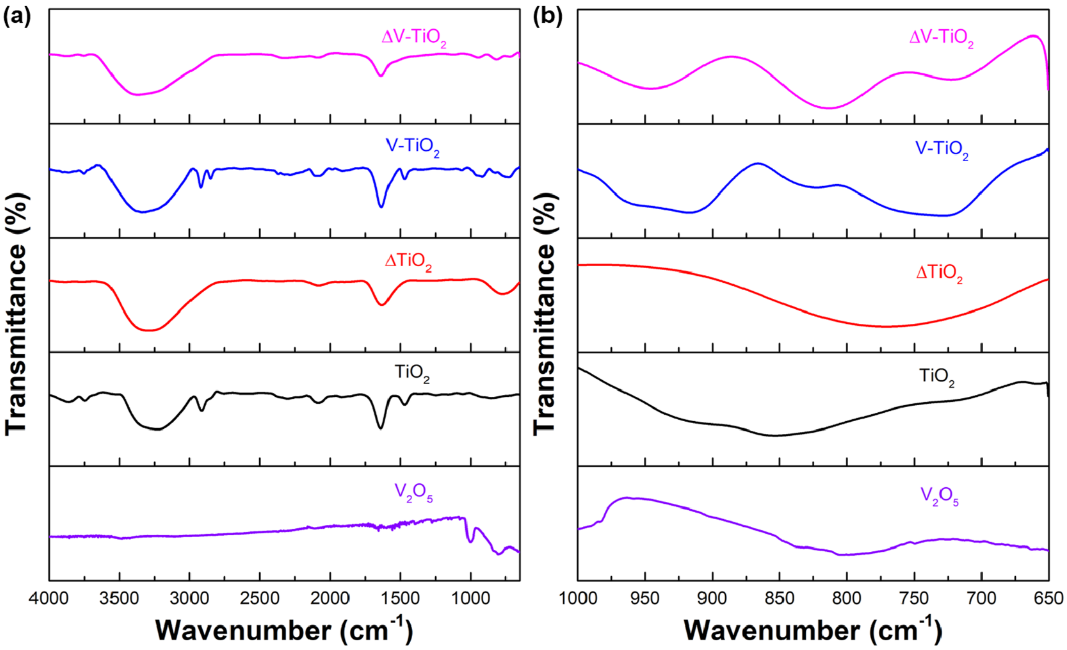

Figure 3: FTIR spectra of (a) pristine V_2O_5, as-prepared (TiO_2, V–TiO_2) and calcined (ΔTiO_2, ΔV-TiO_2) photocatalysts. (b) Magnified view of FTIR spectra in <1,000 cm^{-1} range.

and band gap remain consistent with V doped anatase TiO_2, confirming the spectrum corresponds to ΔV-TiO_2. Tauc's relations were plotted from the obtained absorption data using the following Equation (3).

$$(\alpha h\nu)^n = K(h\nu - E_g) \tag{3}$$

Here, α is the absorption coefficient, h is Planck's constant, ν is the frequency, K is the probability parameter for the transition, E_g is the optical band gap, and the value of n is equivalent to two for a direct band gap. A graph was plotted between $(\alpha h \nu)^2$ and energy, and extrapolation of the linear portion of the curves gives the optical band gap value of pristine V_2O_5 and the prepared photocatalysts,[37] as shown in Figure 4. The calculated band gap value for the pristine V_2O_5 was 3.7 eV. As a result of V doping in TiO_2, there is a reduction in the band gap. The heated and doped samples showed better results due to the removal of impurities and reduction in the distance between the conduction and valence bands. Calculated band gap for TiO_2, ΔTiO_2, V–TiO_2 and ΔV-TiO_2 were 3.22, 3.23, 3.16, and 3.13 eV, respectively having a mean standard deviation of ±0.04 eV.

3.5 Photodegradation of MB

The degradation of the pollutant by the photocatalysts was studied under UV radiation and in the presence of sunlight. For this purpose, the photocatalytic efficiency of the as-prepared and calcined samples was evaluated by measuring the absorption spectra of a methylene blue solution over 90 min exposure to UV light and sunlight, respectively. Figure 5(a–d) shows the results of the degradation of MB by the samples under exposure to UV light. When the photocatalysts were added, the dye discoloration started after some time. During the photocatalytic process, hydroxyl radicals are produced, which cause the degradation of the dye.[38] The added catalyst boosts the rate of degradation, which increases along with the irradiation time.

Table 1 shows the results obtained from the photocatalysis experiment under UV light. It was observed that the doped samples (V–TiO_2 and ΔV-TiO_2) showed better degradation efficiency than the undoped samples (TiO_2, ΔTiO_2). The doping of the crystal structure of TiO_2 by V is reducing the band gap by creating impurity energy levels between the valence and conduction band. Holes are generated in the VB when electrons are shifted to the CB, thereby hindering the recombination of the electron-hole pair. The reaction kinetics of the samples were also studied. The R^2 value of the samples was obtained from plotting the $k\ t = -\ln(C_t/C_o)$ against the time graph as shown in Figure 5(e–h). The results showed that both the as-prepared and the calcined samples followed pseudo-first-order kinetics in accordance with the Langmuir-Hinshelwood model [39] when exposed to UV light. The slope of the graph gives the value of the rate constants. The best photocatalytic performance was of

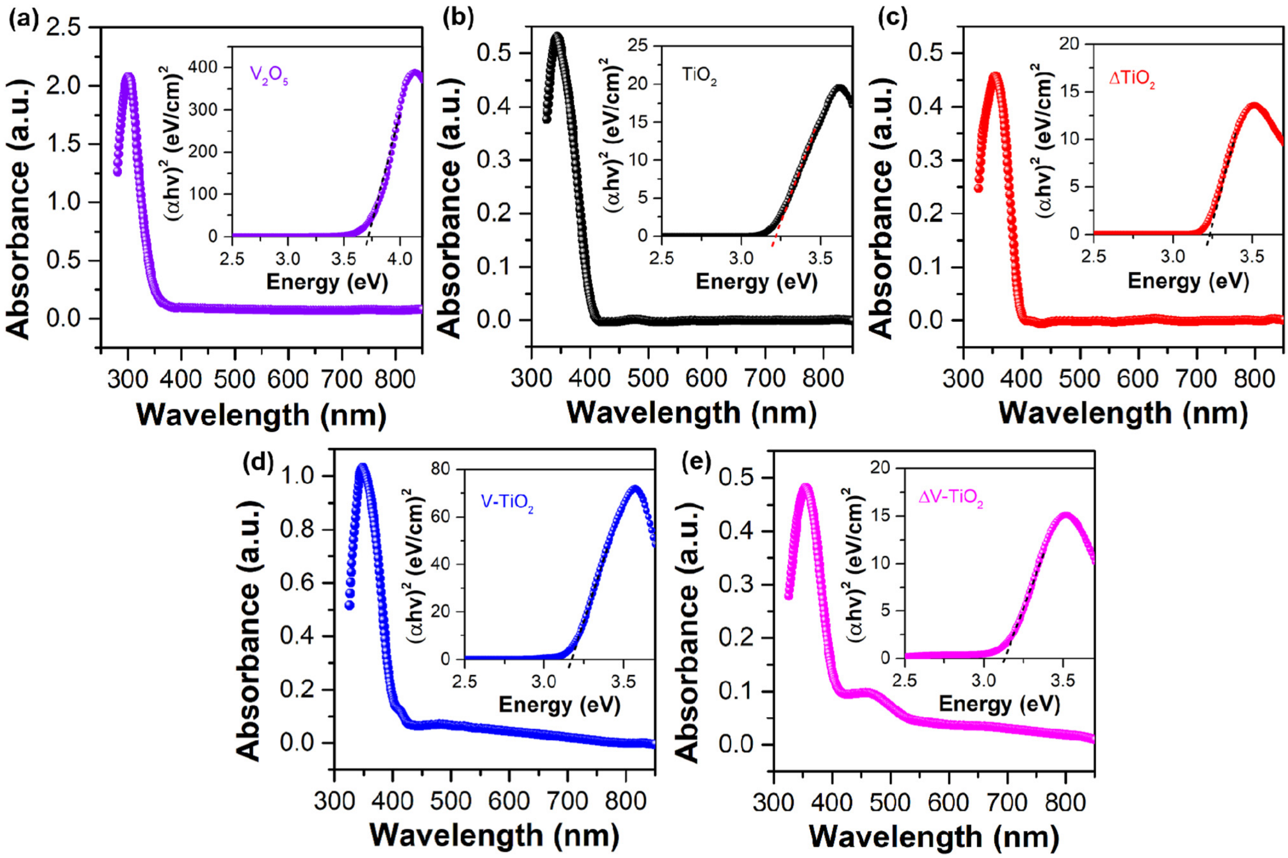

Figure 4: UV/vis spectra and the respective tauc plots of (a) pristine V_2O_5 (b) TiO_2, (c) ΔTiO_2, (d) V–TiO_2, and (e) ΔV-TiO_2 photocatalysts.

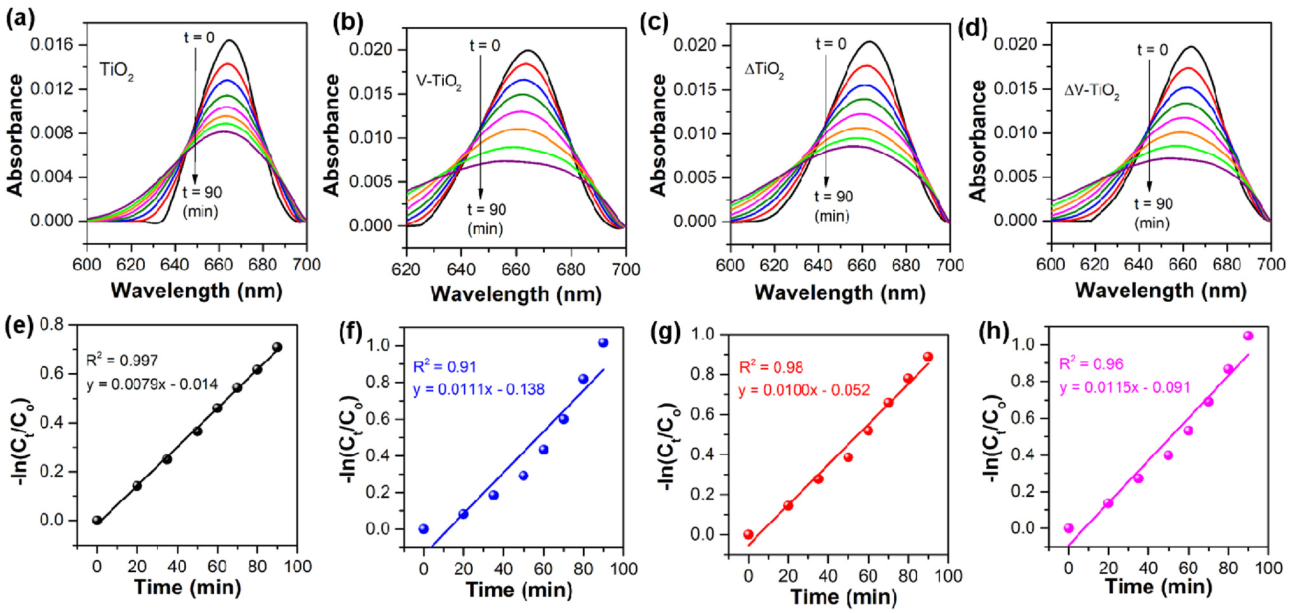

Figure 5: Photocatalytic degradation of methylene blue under UV radiation. (a–d) Photodegradation efficiency of methylene blue over time by as-prepared (TiO_2, V-TiO_2) and calcined (ΔTiO_2, ΔV-TiO_2) photocatalysts. (e–h) Corresponding pseudo-first-order kinetic plots for the photodegradation reaction.

Table 1: Results obtained from the photodegradation of methylene blue by as-prepared (TiO$_2$, V–TiO$_2$) and calcined (ΔTiO$_2$, ΔV-TiO$_2$) photocatalysts under UV light for an exposure time of 90 min.

Photocatalytic activity (under UV)	Dye degradation (%)	Reaction kinetics	Band gap energy (eV)	Rate constant *k* (min^{-1})	R^2
TiO$_2$	51	Pseudo-first-order	3.22	7.91×10^{-3}	0.99
V–TiO$_2$	64		3.16	1.12×10^{-2}	0.91
ΔTiO$_2$	59		3.23	1.01×10^{-2}	0.98
ΔV-TiO$_2$	65		3.13	1.15×10^{-2}	0.96

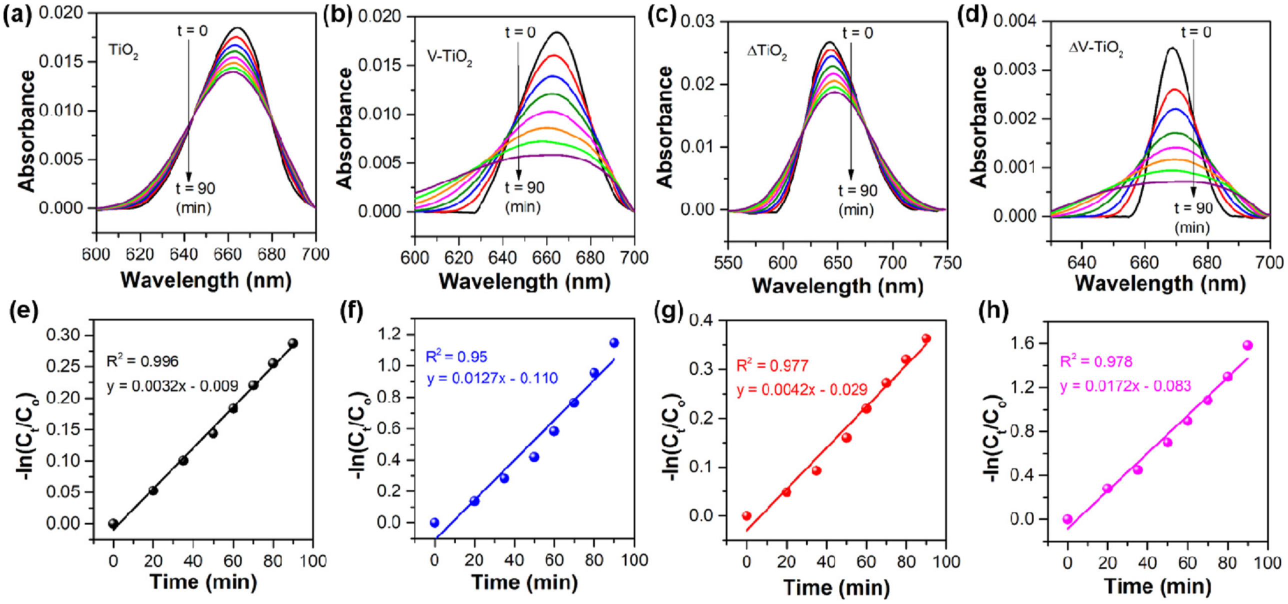

Figure 6: Photocatalytic degradation of methylene blue under sunlight. (a–d) Photodegradation efficiency of methylene blue over time by as-prepared (TiO$_2$, V-TiO$_2$) and calcined (ΔTiO$_2$, ΔV-TiO$_2$) photocatalysts. (e–h) Corresponding pseudo-first-order kinetic plots for the photodegradation reaction.

ΔV-TiO$_2$, showing 65 % degradation of the dye under UV light in 90 min. The R^2 value was 0.96, which also shows that the process follows pseudo-first-order kinetics. The value of the rate constant was 1.15×10^{-2} per min, which was greater than that of the other samples. The order of reactivity of the prepared samples was TiO$_2$ < ΔTiO$_2$ < V–TiO$_2$ < ΔV-TiO$_2$. Both temperature and doping had their separate effects on the properties of the photocatalysts.

Similarly, the efficiency of the photocatalysts was also studied under sunlight by measuring the absorption spectra of MB after an irradiation time of 90 min, as shown in Figure 6(a–d). It was observed that the best photocatalytic performance was shown by the doped samples as compared to the pristine TiO$_2$. The results obtained from the photocatalysis experiment under sunlight are recorded in Table 2.

Pristine TiO$_2$ degraded 25 % of the dye within 90 min. The degradation process was slow because pure TiO$_2$ does not show absorption in visible light due to the high band gap and the high recombination rate. The lower photocatalytic efficiency due to a higher recombination rate of photogenerated electron-hole pairs, has been widely reported in the literature to suppress photocatalytic activity in TiO$_2$ based systems.[40,41] For this reason, doping of vanadium was done to increase the working efficiency of titania in the visible region. Hence, V–TiO$_2$ showed 68 % degradation of the dye as shown in Figure 6(b). The rate of degradation in the calcined samples was faster than in the as-prepared samples due to the removal of impurities like residual organics and surface adsorbates during calcination, which improved crystallinity and enhanced charge transfer. The calcined ΔV-TiO$_2$ showed 80 % degradation of MB within 90 min of irradiation time. The V doping in titania, along with calcination, increases the rate of degradation due to a lowering of band gap energy. This may also lead to a lower recombination rate of e^-/h^+ pairs.

Table 2: Results obtained from the photodegradation of methylene blue by as-prepared (TiO_2, V–TiO_2) and calcined (ΔTiO_2, ΔV-TiO_2) photocatalysts under sunlight for an exposure time of 90 min.

Photocatalytic activity (under sunlight)	Dye degradation	Reaction kinetics	Band gap energy (eV)	Rate constant k (min^{-1})	R^2
TiO_2	25	Pseudo-first-order	3.22	3.25×10^{-3}	0.996
V–TiO_2	68		3.16	1.27×10^{-2}	0.95
ΔTiO_2	30		3.23	4.23×10^{-3}	0.977
ΔV-TiO_2	80		3.13	1.719×10^{-2}	0.978

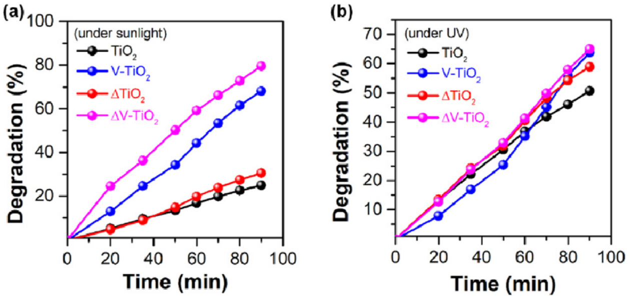

Figure 7: Comparison of the photocatalytic degradation efficiency. (a) Percentage degradation efficiency of as-prepared (TiO_2, V-TiO_2) and calcined (ΔTiO_2, ΔV-TiO_2) photocatalysts under sunlight. (b) Percentage degradation efficiency of the same photocatalysts under UV light.

The reaction kinetics of all the samples were also studied by measuring the R^2 value, using a $-\ln(C_t/C_o)$ versus time graph as shown in Figure 6(e–h). The R^2 value of the calcined ΔV-TiO_2 was 0.98, which proved that this degradation followed pseudo-first-order kinetics. The slope of the graph gives the value of the rate constant, which was 1.719×10^{-2} min^{-1}. This showed that the rate of degradation of the dye was 4 times greater than ΔTiO_2, making it the most efficient photocatalyst among all the prepared samples. The efficiency order was the same as given in the degradation of the dye under UV light.

The graphs showing the percentage degradation are also presented in Figure 7(a and b). A comparison of various doped metal oxides and their photocatalytic performance in the elimination of organic pollutants is shown in Table 3.

3.6 Mechanism of photocatalysis

Vanadium-doped TiO_2 shows enhanced photocatalytic performance compared to pure TiO_2 because the presence of vanadium restricts the recombination of electrons and holes under visible light. Figure 8 shows the mechanism involved in the degradation process. When visible or UV light is present, electrons are stimulated from the valence band to the conduction band of V–TiO_2, which causes a hole to develop in the valence band.[49] After doping with V^{5+}, these photo-generated electrons are trapped in the V^{5+} centers and convert them to V^{4+}, preventing them from recombining with holes; otherwise, these photo-generated electrons can recombine, and only a tiny percentage of them will contribute to the photocatalytic activity and reduce it. The trapped or free photo-generated electrons interact with oxygen to form superoxide anions [50] ($O_2^{\bullet -}$), which then react with water to produce ·OOH radicals. Two molecules of ·OOH

Table 3: A comparison of various doped metal oxides and their performance in the photodegradation of organic contaminants in wastewater.

Photocatalyst	Pollutant	Source	Irradiation time (min)	Degradation (%)	Rate constant k (min^{-1})	Ref.
Cr–Ti oxides	Methylene blue	UV/Vis	240	70	5.2×10^{-3}	[42]
V–SnO_2	Methylene blue	UV	120	70	0.035	[43]
Fe–TiO_2	Methylene blue	Vis	180	99.5	–	[44]
TiO_2–ZrO_2	Rhodamine B	Vis	180	90	0.013	[45]
Fe_3O_4–TiO_2	Methylene blue	Vis	60	75	–	[46]
ZnO	Azo-dye (Acid Brown 14)	Vis	360	100	1.49×10^{-2}	[47]
H_2O_2–TiO_2	Phenol	UV	60	99.2	0.078	[48]
Cu–TiO_2	Acetone	UV/vis	140	86.2	–	[11]
Ce–TiO_2	Methylene blue	Sunlight	90	60	1.06×10^{-2}	[12]
V–TiO_2	Phenol	UV	180	100	–	[13]
V–TiO_2	Trichloroethylene	UV	150	72	1.57×10^{-2}	[14]
V–ZrO_2	Methylene blue	Vis	150	100	–	[15]
ΔV-TiO_2	Methylene blue	Sunlight	90	80	1.72×10^{-2}	This work

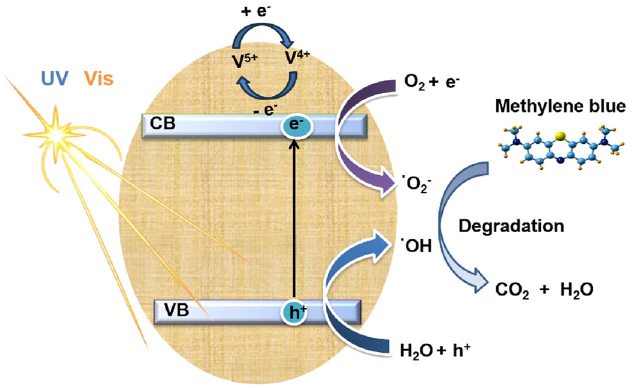

Figure 8: A schematic presentation of the mechanism involved in the degradation of methylene blue by as-prepared (TiO_2, V–TiO_2) and calcined (ΔTiO_2, ΔV-TiO_2) photocatalysts under UV and sunlight.

combine to form H_2O_2, which eventually leads to the formation of hydroxyl radicals(·OH).[51]

$$V - \mathrm{TiO_2} + \mathrm{hv}\ (\mathrm{hv} \geq E_g) \rightarrow V - \mathrm{TiO_2}\ (h^+_{\mathrm{VB}} + e^-_{\mathrm{CB}})$$

$$V^{5+} + e^- \leftrightarrows V^{4+}$$

Trapped or free CB electron reduce molecular oxygen to form superoxide.

$$V^{4+} + O_2 \rightarrow V^{5+} + O_2^{\cdot-}\ ;\ O_2 + e^- \rightarrow O_2^{\cdot-}$$

$$H^+ + O_2^{\cdot-} \rightarrow {}^{\cdot}\mathrm{OOH}$$

$$2\,{}^{\cdot}\mathrm{OOH} \rightarrow H_2O_2 + O_2$$

$$H_2O_2 + \mathrm{e}^- \rightarrow {}^{\cdot}\mathrm{OH} + \mathrm{OH}^-$$

On the other hand, the jumping of electrons into the conduction band leaves behind holes in the valence band. V^{5+} entraps the photogenerated electrons and prevents them from recombining with the holes. These holes react with adsorbed H_2O on their surface to form hydroxyl radicals (•OH).[52,53]

$$V^{5+} + \mathrm{e}^-_{\mathrm{CB}} \rightarrow V^{4+}$$

$$h^+_{\mathrm{VB}} + H_2O/\mathrm{OH}^- \rightarrow {}^{\cdot}\mathrm{OH} + H^+$$

The •OH and $O_2^{\bullet\,-}$ are known as active species,[54] which readily react with a dye to form unstable intermediates that decompose to form the final products (CO_2 and H_2O).

$$\mathrm{O}_2^{\cdot-} + \mathrm{MB\ Dye} \rightarrow \mathrm{demethylated/intermediate\ products} \rightarrow \mathrm{CO_2} + H_2O$$

$${}^{\cdot}\mathrm{OH} + \mathrm{MB\ Dye} \rightarrow \mathrm{demethylated/intermediate\ products} \rightarrow \mathrm{CO_2} + H_2O$$

4 Conclusions

In this work, flower-like assemblies of V-doped TiO_2 microneedles were synthesized via a simple and cost-effective sol-gel method for the removal of organic dyes from wastewater. These samples were calcined at 450 °C for 3–4 h in order to remove any residual organics and surface adsorbates and bring further crystallinity to the structure. Structural and functional group characterization of these samples was carried out by XRD, FTIR, and SEM. The band gap energy was determined using UV/vis spectroscopy, which confirmed that the samples have a low band gap, making them an effective photocatalyst. The photocatalytic efficiency of the prepared samples was studied both under UV light and sunlight for an irradiation time of 90 min. It was found that V-doped TiO_2 showed better efficiency than the undoped samples, both in calcined and pre-heated forms. This is likely due to the reduced band gap and the low recombination rate of e^-/h^+pairs.

Acknowledgment: Adeel Afzal thanks Prof. Dr. Ather F. Khan (CUI, Lahore Campus) for providing XRD results and fruitful discussions on structure elucidation.

Research ethics: Not applicable.

Informed consent: Not applicable.

Author contributions: Tehzeeb Sawaira: Data curation, investigation, methodology, validation. **Amna Jamil:** Data curation, investigation, methodology. **Zuraiz Ahmad Khan:** Formal analysis, validation, and writing – original draft. **Ahsan Sharif**: Formal analysis, resources. **Maha Alruwaili:** Validation, writing – review and editing. **Asghar Ali:** Conceptualization, investigation, methodology. **Adeel Afzal:** Conceptualization, project administration, resources, supervision, and writing – review and editing. All authors have accepted responsibility for the entire content of this manuscript and approved its submission.

Use of Large Language Models, AI and Machine Learning Tools: None declared.

Conflict of interest: The authors declare no conflict of interest.

Research funding: None declared.

Data availability: The data that support the findings of this study are available from the corresponding author, Adeel Afzal, upon reasonable request.

References

1. Ali, E. B.; Shayanmehr, S.; Radmehr, R.; Amfo, B.; Awuni, J. A.; Gyamfi, B. A.; Agbozo, E. Exploring the Impact of Economic Growth on

Environmental Pollution in South American Countries: How does Renewable Energy and Globalization Matter? *Environ. Sci. Pollut. Res.* **2023**, *30*, 15505–15522.

2. Lin, L.; Yang, H.; Xu, X. Effects of Water Pollution on Human Health and Disease Heterogeneity: a Review. *Front. Environ. Sci.* **2022**, *10* (16 pages), 880246.
3. Ahmed, J.; Thakur, A.; Goyal, A. Chapter 1: Industrial Wastewater and its Toxic Effects in *Biological Treatment of Industrial Wastewater*. In *Chemistry in the Environment*; Shah, M. P., Ed.; Royal Society of Chemistry: London, 2021; p 420.
4. Khan, I.; Saeed, K.; Zekker, I.; Zhang, B.; Hendi, A. H.; Ahmad, A.; Ahmad, S.; Zada, N.; Ahmad, H.; Shah, L. A.; Shah, T.; Khan, I. Review on Methylene Blue: Its Properties, Uses, Toxicity and Photodegradation. *Water* **2022**, *14*, 242 (30 pages).
5. Krishna Moorthy, A.; Govindarajan Rathi, B.; Shukla, S. P.; Kumar, K.; Shree Bharti, V. Acute Toxicity of Textile Dye Methylene Blue on Growth and Metabolism of Selected Freshwater Microalgae. *Environ. Toxicol. Pharmacol.* **2021**, *82*, 103552 (9 pages).
6. Din, M. I.; Khalid, R.; Najeeb, J.; Hussain, Z. Fundamentals and Photocatalysis of Methylene Blue Dye Using Various Nanocatalytic Assemblies – a Critical Review. *J. Cleaner Prod.* **2021**, *298*, 126567 (18 pages).
7. Oladoye, P. O.; Ajiboye, T. O.; Omotola, E. O.; Oyewola, O. J. Methylene Blue Dye: Toxicity and Potential Elimination Technology from Wastewater. *Results Eng.* **2022**, *16*, 100678 (17 pages).
8. Waghchaure, R. H.; Adole, V. A.; Jagdale, B. S. Photocatalytic Degradation of Methylene Blue, Rhodamine B, Methyl Orange and Eriochrome Black T Dyes by Modified ZnO Nanocatalysts: A Concise Review. *Inorg. Chem. Commun.* **2022**, *143*, 109764 (15 pages).
9. Hamed, N. K. A.; Ahmad, M. K.; Hairom, N. H. H.; Faridah, A. B.; Mamat, M. H.; Mohamed, A.; Suriani, A. B.; Soon, C. F.; Fazli, F. I. M.; Mokhtar, S. M.; Shimomura, M. Photocatalytic Degradation of Methylene Blue by Flowerlike Rutile-phase TiO2 Film Grown via Hydrothermal Method. *J. Sol-Gel Sci. Technol.* **2022**, *102*, 637–648.
10. Liang, Y.; Chen, S.; Zhong, J.; Ding, H.; Zhu, Z.; Li, S. Acid-Etched Coal Fly Ash/TiO2 Nanocomposites with High Photocatalytic Degradation Efficiency: a High Value-Added Application of Coal Fly Ash. *J. Sol-Gel Sci. Technol.* **2022**, *103*, 185–194.
11. Degefu, D. M.; Liao, Z. Photocatalytic Degradation of Volatile Organic Compounds Using Nanocomposite of P-type and N-type Transition Metal Semiconductors. *J. Sol-Gel Sci. Technol.* **2021**, *98*, 605–614.
12. Jamil, A.; Sawaira, T.; Ali, A.; Awais, M.; Habib, A.; Hussain, T.; Sharif, A.; Iqbal, N.; Afzal, A. Ce-TiO2 Nanoparticles with Surface-Confined Ce3+/Ce4+ Redox Pairs for Rapid Sunlight-Driven Elimination of Organic Contaminants from Water. *Environ. Nanotechnol.; Monit. Manage.* **2024**, *21*, 100946 (9 pages).
13. Rossi, L.; Palacio, M.; Villabrille, P. I.; Rosso, J. A. V-Doped TiO2 Photocatalysts and their Application to Pollutant Degradation. *Environ. Sci. Pollut. Res.* **2021**, *28*, 24112–24123.
14. Nguyen, D. M.; Ding, S.; Nghiem, T. T.; Nguyen, V. A.; Mejía, E. Visible Light-Driven Degradation of Trichloroethylene in Aqueous Phase with Vanadium-Doped TiO2 Photocatalysts. *Sol. RRL* **2023**, *7*, 2200938 (10 pages).
15. Wahba, M. A.; Yakout, S. M. Innovative Visible Light Photocatalytic Activity for V-Doped ZrO2 Structure: Optical, Morphological, and Magnetic Properties. *J. Sol-Gel Sci. Technol.* **2019**, *92*, 628–640.
16. Yao, W.; Luo, C.; Wu, J.; Hou, G. Degradation of Acid Yellow 36 Azo Dye from Textile Wastewater Using Vanadium-Doped TiO2 Photonanocatalyst. *Int. J. Electrochem. Sci.* **2022**, *17*, 220916 (14 pages).
17. Wu, K.-J.; Tse, E. C. M.; Shang, C.; Guo, Z. Nucleation and Growth in Solution Synthesis of Nanostructures – from Fundamentals to Advanced Applications. *Prog. Mater. Sci.* **2022**, *123*, 100821 (43 pages).
18. Zhu, T.; Li, J.; Wu, Q. Construction of TiO2 Hierarchical Nanostructures from Nanocrystals and their Photocatalytic Properties. *ACS Appl. Mater. Interfaces* **2011**, *3*, 3448–3453.
19. Han, W.; Ge, X.; Yuan, J.; Pan, R.; Yang, Y.; Zou, G.; Xie, H. Spatial-Confined Effect of CuOx Microneedles Bundles on TiO2 Nanotubes: Reinforcing the Adsorption and Enrichment of Ultralow Concentration Nitrate for Efficient NH3 Electrosynthesis. *Appl. Catal. B Environ. Energy* **2025**, *361*, 124659 (11 pages).
20. Deng, A.; Zhu, Y.; Guo, X.; Zhou, L.; Jiang, Q. Synthesis of Various TiO2 Micro-/Nano-Structures and their Photocatalytic Performance. *Materials* **2018**, *11*, 995 (11 pages).
21. Kamat, P. V. Meeting the Clean Energy Demand: Nanostructure Architectures for Solar Energy Conversion. *J. Phys. Chem. C*, *111*, **2007**, 2834–2860.
22. Yu, J.; Low, J.; Xiao, W.; Zhou, P.; Jaroniec, M. Enhanced Photocatalytic CO2-Reduction Activity of Anatase TiO2 by Coexposed {001} and {101} Facets. *J. Am. Chem. Soc.* **2014**, *136*, 8839–8842.
23. Lu, Z.; Duan, J.; He, L.; Hu, Y.; Yin, Y. Mesoporous TiO2 Nanocrystal Clusters for Selective Enrichment of Phosphopeptides. *Anal. Chem.* **2010**, *82*, 7249–7258.
24. Fan, Q.; Wang, T.; Fan, W.; Xu, L. Recyclable Visible-Light Photocatalytic Composite Materials Based on Tubular Au/TiO2/SiO2 Ternary Nanocomposites for Removal of Organic Pollutants from Water. *Compos. Commun.* **2022**, *32*, 101154 (5 pages).
25. Kosta, I.; Navone, Ch.; Bianchin, A.; García-Lecina, E.; Grande, H.; Mouko, H. I.; Azpeitia, J.; García, I. Influence of Vanadium Oxides Nanoparticles on Thermoelectric Properties of an N-type Mg2Si0.888Sn0.1Sb0.012 Alloy. *J. Alloys Compd.* **2021**, *856*, 158069 (8 pages).
26. Abd-Alghafour, N. M.; Ahmed, N. M.; Hassan, Z.; Almessiere, M. A. Hydrothermal Synthesis and Structural Properties of V2O5 Nanoflowers at Low Temperatures. *J. Phys. Conf. Ser.* **2018**, *1083*, 012036 (7 pages).
27. Liu, H.; Wu, Y.; Zhang, J. A New Approach Toward Carbon-Modified Vanadium-Doped Titanium Dioxide Photocatalysts. *ACS Appl. Mater. Interfaces* **2011**, *3*, 1757–1764.
28. Monshi, A.; Foroughi, M. R.; Monshi, M. R. Modified Scherrer Equation to Estimate More Accurately Nano-Crystallite Size Using XRD. *World J. Nano Sci. Eng.* **2012**, *2*, 154–160.
29. Rathore, N.; Kulshreshtha, A.; Shukla, R. K.; Sharma, D. Study on Morphological, Structural and Dielectric Properties of Sol-Gel Derived TiO2 Nanocrystals Annealed at Different Temperatures. *Phys. B: Condensed Matter* **2020**, *582*, 411969 (7 pages).
30. Zhou, W.; Liu, Q.; Zhu, Z.; Zhang, J. Preparation and Properties of Vanadium-Doped TiO2 Photocatalysts. *J. Phys. D: Appl. Phys.* **2010**, *43*, 035301 (7 pages).
31. Bukit, B. F.; Frida, E.; Humaidi, S.; Sinuhaji, P. Preparation and Characterization of CTAB Surfactant Modified TiO2 Nanoparticles as Antibacterial Fabric Coating Material. *J. Phys. Conf. Ser.* **2022**, *2165*, 012022 (8 pages).
32. Lashari, Z. A.; Lalji, S. M.; Ali, S. I.; Kumar, D.; Khan, B.; Tunio, U. Physiochemical Analysis of Titanium Dioxide and Polyacrylamide Nanofluid for Enhanced Oil Recovery at Low Salinity. *Chem. Pap.* **2024**, *78*, 3629–3637 (9 pages).
33. Ibrahim, I.; Belessiotis, G. V.; Arfanis, M. K.; Athanasekou, C.; Philippopoulos, A. I.; Mitsopoulou, C. A.; Romanos, G. E.; Falaras, P.

Surfactant Effects on the Synthesis of Redox Bifunctional V2O5 Photocatalysts. *Materials* **2020**, *13*, 4665 (13 pages).

34. Wei, Y.; Ryu, C.-W.; Kim, K.-B. Improvement in Electrochemical Performance of V2O5 by Cu Doping. *J. Power Sources* **2007**, *165*, 386–392.
35. Aydın, M. T. A.; Hoşgün, H. L. Hydrothermal Synthesis and Characterization of Vanadium-Doped Titanium Dioxide Nanotubes. *J. Aust. Ceram. Soc.* **2020**, *56*, 645–651.
36. Tanabe, I.; Ozaki, Y. Far- and Deep-Ultraviolet Spectroscopic Investigations for Titanium Dioxide: Electronic Absorption, Rayleigh Scattering, and Raman Spectroscopy. *J. Mater. Chem. C* **2016**, *4*, 7706–7717.
37. Javaid, A.; Imran, M.; Kanwal, F.; Latif, S.; Erben, M. F.; Noureen, S. Structural, Optical and Morphological Investigation of Bismuth Substituted Cerium Ferrite: An Efficient Photocatalyst and Dielectric Material for Various Applications. *Mater. Chem. Phys.* **2022**, *291*, 126704 (13 pages).
38. Waseem, S.; Saleem, H.; Akhtar, M. N.; Imran, M.; Javaid, A.; AlDamen, M. A.; Bikas, R.; Khanfar, M. A. A Zn-Based Zig-Zag 1D Chain Type Coordination Polymer for Removal of Methylene Blue Dye from an Aqueous Solution. *Inorg. Chim. Acta* **2024**, *559*, 121756 (9 pages).
39. Wu, C.-H.; Chern, J.-M. Kinetics of Photocatalytic Decomposition of Methylene Blue. *Ind. Eng. Chem. Res.* **2006**, *45*, 6450–6457.
40. Umebayashi, T.; Yamaki, T.; Itoh, H.; Asai, K. Analysis of Electronic Structures of 3d Transition Metal-Doped TiO2 Based on Band Calculations. *J. Phys. Chem. Solids* **2002**, *63*, 1909–1920.
41. Lin, W.-C.; Lin, Y.-J. Effect of Vanadium(IV)-Doping on the Visible Light-Induced Catalytic Activity of Titanium Dioxide Catalysts for Methylene Blue Degradation. *Environ. Eng. Sci.* **2012**, *29*, 447–452.
42. Rauf, M. A.; Meetani, M. A.; Khaleel, A.; Ahmed, A. Photocatalytic Degradation of Methylene Blue Using a Mixed Catalyst and Product Analysis by LC/MS. *Chem. Eng. J.* **2010**, *157*, 373–378.
43. Soltan, W. B.; Lassoued, M. S.; Ammar, S.; Toupance, T. Vanadium Doped SnO2 Nanoparticles for Photocatalytic Degradation of Methylene Blue. *J. Mater. Sci.: Mater. Electron.* **2017**, *28*, 15826–15834.
44. Anwar, D. I.; Mulyadi, D. Synthesis of Fe-TiO2 Composite as a Photocatalyst for Degradation of Methylene Blue. *Procedia Chem* **2015**, *17*, 49–54.
45. Abdi, J.; Yahyanezhad, M.; Sakhaie, S.; Vossoughi, M.; Alemzadeh, I. Synthesis of Porous TiO2/ZrO2 Photocatalyst Derived from Zirconium Metal Organic Framework for Degradation of Organic Pollutants Under Visible Light Irradiation. *J. Environ. Chem. Eng.* **2019**, *7*, 103096 (9 pages).
46. Djellabi, R.; Yang, B.; Adeel Sharif, H. M.; Zhang, J.; Ali, J.; Zhao, X. Sustainable and Easy Recoverable Magnetic TiO2-Lignocellulosic Biomass@Fe3O4 for Solar Photocatalytic Water Remediation. *J. Cleaner Prod.* **2019**, *233*, 841–847.
47. Sakthivel, S.; Neppolian, B.; Shankar, M. V.; Arabindoo, B.; Palanichamy, M.; Murugesan, V. Solar Photocatalytic Degradation of Azo Dye: Comparison of Photocatalytic Efficiency of Zno and TiO2. *Sol. Energy Mater. Sol. Cells* **2003**, *77*, 65–82.
48. Akbal, F.; Nur Onar, A. Photocatalytic Degradation of Phenol. *Environ. Monit. Assess.* **2003**, *83*, 295–302.
49. Le, H. A.; Linh, L. T.; Chin, S.; Jurng, J. Photocatalytic Degradation of Methylene Blue by a Combination of TiO2-Anatase and Coconut Shell Activated Carbon. *Powder Technol*. **2012**, *225*, 167–175.
50. Wang, G.; Wu, F.; Zhang, X.; Luo, M.; Deng, N. Enhanced TiO2 Photocatalytic Degradation of Bisphenol E by β-Cyclodextrin in Suspended Solutions. *J. Hazard. Mater.* **2006**, *133*, 85–91.
51. Nguyen, C. H.; Fu, C.-C.; Juang, R.-S. Degradation of Methylene Blue and Methyl Orange by Palladium-Doped TiO2 Photocatalysis for Water Reuse: Efficiency and Degradation Pathways. *J. Cleaner Prod.* **2018**, *202*, 413–427.
52. Amreetha, S.; Dhanuskodi, S.; Nithya, A.; Jothivenkatachalam, K. Three Way Electron Transfer of a C–N–S Tri Doped Two-phase Junction of TiO2 Nanoparticles for Efficient Visible Light Photocatalytic Dye Degradation. *RSC Adv*. **2016**, *6*, 7854–7863.
53. Hu, Y.; Song, X.; Jiang, S.; Wei, C. Enhanced Photocatalytic Activity of Pt-Doped TiO2 for No*x* Oxidation Both Under UV and Visible Light Irradiation: a Synergistic Effect of Lattice Pt4+ and Surface PtO. *Chem. Eng. J.* **2015**, *274*, 102–112.
54. Lü, C.-N.; Chen, M.-M.; Zhang, W.-H.; Li, D.-X.; Dai, M.; Lang, J.-P. Construction of Zn(II) and Cd(II) Metal–Organic Frameworks of Diimidazole and Dicarboxylate Mixed Ligands for the Catalytic Photodegradation of Rhodamine B in Water. *CrystEngComm* **2015**, *17*, 1935–1943.